

Raman scattering from the CaC_6 superconductor in the presence of disorder

A. Mialitsin¹, J. S. Kim², R. K. Kremer² and G. Blumberg¹

¹*Department of Physics and Astronomy, Rutgers University, Piscataway, New Jersey 08854-8019, USA*

²*Max-Planck-Institut für Festkörperforschung, 70569 Stuttgart, Germany*

(Dated: November 19, 2018)

Polarized Raman scattering has been performed on CaC_6 superconductor. We identify two of the three Raman active E_g phonon modes at 440 and 1508 cm^{-1} expected for the $R\bar{3}m$ space group of CaC_6 . These first order scattering modes appear along with the D and G bands around 1300 cm^{-1} and 1600 cm^{-1} that are similar in origin to the corresponding bands in plain graphite. The intensities of the D and G bands in CaC_6 correlate with degree of disorder. The D band arises from the double resonant Raman scattering process; its frequency shifts as a function of excitation energy with $\sim 35 \text{ cm}^{-1}/\text{eV}$. The double resonant Raman scattering probes phonon excitations with finite wave vector q . We estimate the characteristic spacing of structural defects to be on the scale of about 100 Å by comparing the intensity of the D band and the 1508 cm^{-1} E_g mode in CaC_6 to calibrated intensity ratio of analogous bands in disordered graphites. A sharp superconducting coherence peak at 24 cm^{-1} is observed below T_c .

PACS numbers: 71.20.Tx, 74.25.Gz, 74.25.Kc, 78.30.-j

I. INTRODUCTION

Examples of superconductivity in graphite intercalated with alkali metals have been known for several decades¹. More recently the occurrence of superconductivity in graphite intercalation compounds (GICs) has been linked to the partial occupation of the interlayer band in those intercalated structures that display the superconducting phase transition^{2,3}. Experimental studies of superconductivity in GICs were limited to very low temperatures, since previously known GIC superconductors, like KC_8 or LiC_2 , display low superconducting transition temperatures under ambient conditions. The synthesis of CaC_6 , with a surprisingly high superconducting transition temperature⁴ of 11.5 K, has spurred new research in the area of GIC superconductivity. In addition to encouraging new experiments, this development calls for expanding theoretical models to explain its high T_c . CaC_6 further merits special attention among simple graphite derived compounds because it illustrates how the properties of graphene sheets are altered by the change in crystal symmetry and in electronic band structure due to interaction with the Ca sublattice.

The CaC_6 structure is shown in Fig. 1 a. It belongs to the space group Nr. 166 ($R\bar{3}m$) with an $AgBgCg$ stacking sequence which sets it apart from all other known 1st stage GIC compounds^{5,6}. Here g stands for the hexagonal graphene planes stacked in a *primitive fashion* (as opposed to *staggered* plane stacking of graphite). The unit cell is rhombohedral and spans three intercalate planes. Its inversion center lies in the middle of the graphitic hexagon in the median plane.

Fractional contribution of Ca atoms at the corners of the unit cell adds up to one atom per unit cell.

CaC_6 and its parent graphene structure are intuitively comparable. Introducing Ca atoms inbetween the carbon sheets lowers the symmetry of the D_{6h} space group of graphene to the D_{3d}^5 space group. This leads to a unit cell in CaC_6 with a hexagonal cross-section area in the ab -plane that is three times larger than that of graphene, and a corresponding Brillouin zone (BZ) that is three times smaller. The BZ of graphene and CaC_6 are rotated by 30° in respect to each other, thus when the graphene BZ is folded into that of CaC_6 the equivalent K and K' points fall back onto the Γ point. When comparing the phonon dispersion of graphene and CaC_6 the 21 phonon branches in CaC_6 can be derived approximately from 6 graphene phonon branches folded into the smaller CaC_6 BZ, resulting in $3 \times 6 = 18$ branches, in addition to the three phonon branches from the Ca sublattice.

According to first principles calculations^{7,8}, low frequency Ca vibrations and carbon out-of-plane vibrations both contribute almost equally to most of the electron-phonon coupling responsible for the Cooper pairs binding. Contrary to this finding, however, based on evidence from isotope effect measurements⁹ it was the Ca phonons that have been found to be primarily responsible for the mediation of superconductivity. Lattice vibrations have also been the focus of spectroscopic investigations: a Raman study directed at the zone center phonon modes¹⁰ and an inelastic X-ray (IXR) scattering study aimed at low-energy phonon branches¹¹.

The Raman study has recorded a Raman active band

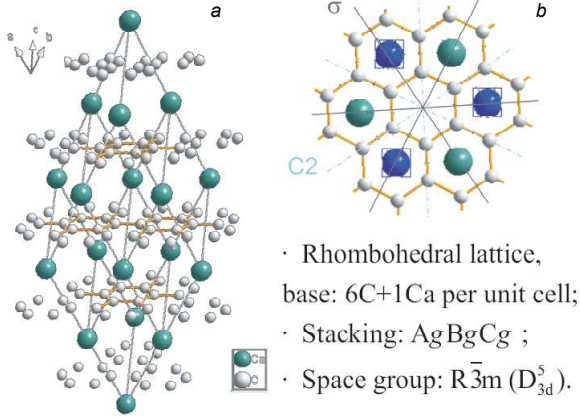


FIG. 1: (color online) Crystal structure of CaC_6 . a) The layered nature of the compound with the intercalant sandwiched between the host graphite planes is shown in a 4 times 4 super cell. b) view on the CaC_6 structure from the top. Thin lines indicate the two-fold rotational axis C_2 and the mirror planes σ . The three-fold rotational axis that coincides with the six-fold rotation-reflection axis goes vertically through the paper at the point of the intersection of the C_2 axes in the central hexagon. Blue colored Ca atoms framed by squares are above the graphene layer and the green colored ones below.

at 1500 cm^{-1} that has been assigned to the high-frequency E_g vibration by a rough Raman shift coincidence with the theoretical prediction⁸. Since the frequency of this band is measured to be higher than 1447 cm^{-1} corresponding to the zone center mode predicted by a 'frozen-phonon' density functional calculation, it has been attempted to explain this discrepancy by non-adiabatic behavior¹². Non-adiabatic effects are assumed to become important when a relatively short lattice vibration period is accompanied by a relatively long electron scattering time¹³. In such a case the Born Oppenheimer approximation (BOA), which asserts that electrons remain in the ground state at all times in the process of the lattice vibration, is not applicable any more and excitations of the electron cloud to higher states as a consequence of electron-phonon coupling need to be considered.

The IXR study has traced two acoustic branches and one optical Ca sublattice branch along the Γ -L and Γ -X directions finding good agreement with predictions by Calandra and Mauri⁸ barring a slight systematic underestimation of calculated band frequencies throughout the dispersion. The energy window of the X-ray study has been limited to energies up to 40 meV and in both works some of the predicted modes have been absent in experimental data. This leaves ample

room for more in depth CaC_6 phonon studies.

Double resonant Raman scattering¹⁴ (DRRS) is a process that involves light scattering mediated by phonon excitations with a quasi-momentum greater than zero¹⁵. DRRS allows to access selected points in the phonon dispersion away from the Γ point. Raman bands associated with DRRS occur in the presence of structural defects which are necessary to ensure quasi-momentum conservation¹⁵. In fact the phonon dispersion of graphite has been investigated by means of DRRS in considerable detail¹⁶. The so-called D band, a disorder induced feature appearing between 1300 cm^{-1} and 1400 cm^{-1} in graphite is also seen in CaC_6 Raman spectra in the same frequency range; however, the underlying mechanism behind DRRS in CaC_6 has not been described. The dispersive behavior of the D band¹⁰ in CaC_6 is a fingerprint signature of DRRS. In the context of DRRS and disorder, Hlinka et al.¹⁰ have highlighted the rapid sample degradation in air. It is apparent that the interpretation of spectroscopic data is affected by sample quality and age.

While the body of work describing superconductivity in CaC_6 is quite substantial, there are discrepancies in the estimations of the magnitude of the SC gap by means of tunneling spectroscopies. The accounts vary from $2\Delta = 21.8\text{ cm}^{-1}$ (Ref.¹⁷) to 37.1 cm^{-1} (Ref.¹⁸). The former value puts superconductivity in CaC_6 into a weak coupling regime while the latter raises the possibility of strong coupling. A third scanning tunneling spectroscopy study (Ref.¹⁹) provides an intermediate value of 25.8 cm^{-1} . This issue has been addressed in Ref.²⁰ by proposing a distribution of gaps around the average value of 26.3 cm^{-1} as calculated from first principles (SCDFT). An optical investigation of reflectance of CaC_6 in far infrared²¹ also suggests a distribution of gaps around the above value.

In this work we study CaC_6 crystals by polarized Raman spectroscopy. We observe expected Raman active E_g vibrational modes at 440 and 1508 cm^{-1} . The disorder induced D band appears $\sim 150\text{-}200\text{ cm}^{-1}$ below the latter E_g mode, accompanied by weaker disorder related bands. We measure Raman spectra with multiple excitations to highlight the dispersive nature of the D band in the DRRS process. The prominent presence of the D band further enables exploration of structural defects in the investigated samples. Electronic Raman scattering reveals a sharp superconducting pair breaking peak appearing at 24 cm^{-1} below T_c . We assess how the degree of disorder correlates with the superconducting properties.

II. EXPERIMENTAL

The high-quality CaC_6 crystals were synthesized by reacting highly oriented pyrolytic graphite (Advanced Ceramics, Grade : ZYA) with a molten alloy of Li and Ca at 350°C for several weeks⁷. The resulting *c*-oriented polycrystalline samples were characterized by X-ray diffraction, and susceptibility measurements. The samples for the Raman study were carefully selected to have almost pure CaC_6 phase with a minimal amount ($< 5\%$) of impurity LiC_x phase, and to show a very sharp superconducting transition ($\Delta T_c(10\% - 90\%) = 0.1 \text{ K}$) with the onset at $T_c = 11.4 \text{ K}$. Further details on the characterization of the samples can be found in Ref.⁶. Because of the sensitivity of the lustrous sample surface to moisture contained in air, the samples have been manipulated and mounted in Argon atmosphere. The samples were then transferred to and cleaved in a He-filled glove box that was enclosing the continuous flow He-cryostat. The freshly cleaved specimen were then immediately cooled to 5 K and hold below 20 K at all times for the duration of the measurement.

To perform Raman scattering from the *ab*-plane of bulk CaC_6 we have used a Kr+ laser for a range of excitation wavelengths with 2 mW power focused to a $50 \times 100 \mu\text{m}$ spot, an Oxford Instruments cryostat for sample temperature control down to 3 K , and a custom triple-stage spectrometer. We have employed circularly polarized light with the optical configurations selecting either the same or opposite chirality. The former and the latter are respectively referred to as Right-Right (RR) and Right-Left (RL) configurations. The circularly polarized configurations allow to record symmetry resolved Raman spectra. For the D_{3d} point group the E_g symmetry is selected in the RL scattering geometry and the $A_{1g} \oplus A_{2g}$ symmetries in the RR setup²². The symmetry channels correspond to irreducible representations of distinctive lattice vibration modes.

III. RAMAN ACTIVE MODES

The atoms in the unit cell that remain unaffected by symmetry operations of the space group determine the characters of the vibrational representation Γ_{vib} . For CaC_6 we find the respective characters to be:

$$\begin{array}{c|cccccc} D_{3d}^5 & T_3 & 2C_3 & 3C_2 & I & 2S_6 & 3\sigma_d \\ \hline \Gamma_{vib} & 21 & 0 & -3 & -3 & 0 & 1 \end{array}$$

The symmetry elements (illustrated by Fig. 1 b) are de-

noted as follows: T_3 - translation, C_3 - three-fold rotation around the axis perpendicular to the graphene plane, C_2 - two-fold rotation around the axes lying in the graphene plane, I - inversion, S_6 - six-fold rotation-reflection around the axis perpendicular to the graphene plane, σ_d - diagonal mirror planes bisecting the angle enclosed by the C_2 axes. With the knowledge of the characters table Γ_{vib} is reduced to the direct sum

$$\Gamma_{vib} = A_{1g} \oplus A_{1u} \oplus 2A_{2g} \oplus 3A_{2u} \oplus 3E_g \oplus 4E_u. \quad (1)$$

One set of $A_{2u} \oplus E_u$ irreducible representations corresponds to the translational degrees of freedom (T_z and T_{xy}) and thus is allocated to the acoustic branches. A second pair of $A_{2u} \oplus E_u$ irreducible representations is attributed to the mutual shift of the Ca and C sublattices¹⁰ comprising the three lowest optical phonon branches (see Fig. 4 c). Modes associated with Ca movement are not Raman active.

Polarized Raman spectra recorded at 5 K from the CaC_6 *ab*-plane are displayed in Fig. 2. It shows Raman bands observed with the 476 nm excitation up to the Raman shift of 1700 cm^{-1} . The two juxtaposed data sets have been obtained in different scattering configurations. The RL geometry with circularly polarized light of opposite chirality for the incident and scattered beams selects Raman modes of the E_g symmetry. The data set collected in RL features a total of six modes in the accessed energy range. The RR geometry with incident and scattered light of the same chirality selects modes of the $A_{1g} \oplus A_{2g}$ symmetries. The data set collected in RR features four bands. Depending on the presence the modes in just the E_g or in both symmetry channels we categorize the observed features as polarized, partially polarized and depolarized.

Resolving polarization is helpful in identifying the modes. We notice that to a large extent the RR polarization spectrum follows the RL spectrum, with the exception of the modes at around 1100 , 1500 and 1600 cm^{-1} and the low energy peak related to superconductivity. Underlying the Raman peaks there is a broad depolarized continuum that is phenomenologically modeled by a broad feature peaking at around 800 cm^{-1} on top of a linear slope. We determine frequencies of the phononic Raman bands in the RL polarization by a fit to a superposition of Raman oscillators²³ and the continuum:

$$\chi'' = \sum_i \frac{A_i \omega_i \gamma_i \omega}{(\omega^2 - \omega_i^2)^2 + (\gamma_i \omega)^2} + cont. \quad , \quad (2)$$

where A_i , γ_i and ω_i are the amplitude, the line width and the Raman shift of the respective peaks. The fitted peak parameters are listed in Table I.

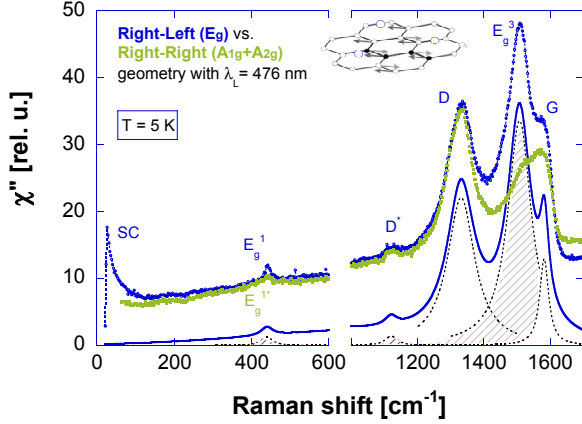


FIG. 2: (color online) Polarized Raman spectra from CaC_6 at 5 K. RR and RL polarizations obtained with the 476 nm excitation. Symbols display experimental data. Blue circles interconnected with a dashed line correspond to the RL geometry and green circles correspond to the RR geometry. The solid line is a fit to E_g data by superposition of five Raman oscillators on a broad continuum. The region between 600 and 1100 cm^{-1} is featureless and has been cropped out.

Only the 1508 cm^{-1} mode is found to be fully polarized (present in the E_g symmetry channel and entirely absent in $A_{1g} \oplus A_{2g}$). This mode is identified as the high frequency doubly degenerate carbon in-plane stretching E_g^3 mode (Fig. 2 inset). The much weaker mode at 440 cm^{-1} appears to be partially polarized. There is a sharp peak present in the E_g symmetry channel superimposed on a broader feature appearing in both polarizations. By examining the phonon dispersion^{7,8} (Fig. 4 c), we identify the additional intensity in RL as the lowest Raman active E_g^1 mode which we measure at 440 cm^{-1} . The origin of depolarized modes, which we associate with DRRS (see section IV), is different from that of polarized modes, which are zone center modes visible due to first order Raman scattering, and is going to be discussed in section IV. We will discuss the graphite like G band at 1600 cm^{-1} that is partially polarized in section VI.

TABLE I: Fit parameters for the CaC_6 Raman spectrum at $T = 5 \text{ K}$ in RL polarization excited with $\lambda_L = 476 \text{ nm}$.

fit parameters \ peaks	E_g^1	D^*	D	E_g^3	G
ω_i [1/cm]	440	1120	1332	1508	1582
γ_i [1/cm]	36	44	100	86	32
A_i [rel. u. $\times 10^{-3}$ /cm]	0.45	0.62	22.1	29.0	4.2

The experimentally measured frequency of the E_g^3 mode at 5 K deviates from the calculated one by 4%. E_g^1 is found to match the frequency of 434 cm^{-1} determined from first principles calculations⁸ more closely with a difference of only 1.5%. The question how and if the renormalization of zone center modes frequencies should scale with mode frequency in the context of first-principles calculations beyond BOA is open for discussion.

As noted above the intensities of the E_g modes vary strongly. The method of zone folding that is commonly used to qualitatively evaluate the phonon dispersions of intercalate compounds¹ is helpful to discuss this fact. The E_g^1 and the E_g^2 modes can be understood as turned on by zone-folding of the pristine primitive graphite phonon dispersion²⁴. In this context, the E_g^1 mode is expected to be weak²⁵ reflecting the observation that the modulation of the carbon layers by Ca atoms is weak. The high frequency E_g^3 mode of CaC_6 (D_{3d}^5 space group) is deduced from the E_{2g} vibration in graphene³⁷ (D_{6h}) and thus is the only true not zone-folded graphitic intra-layer Raman active mode. Accordingly the E_g^3 mode dominates the Raman spectrum in the E_g symmetry channel.

The mode corresponding to E_g^3 is observed to be downshifted in many GICs, sometimes displaying an asymmetric shape attributed to Fano type interaction with the electronic background (see Ref-s^{25,26} for RbC_x and KC_x). While the frequency of the E_g^3 phonon is clearly downshifted in CaC_6 when compared to the parent graphite mode (see Fig. 5 a and c) we observe no asymmetry and fit the mode with a conventional Raman oscillator.

The energy region where the E_g^2 mode is expected (1100 cm^{-1}) displays a depolarized feature. We believe that we observe a disorder induced band instead of the actual zone center mode. The Raman active A_{1g} mode expected around 1380 cm^{-1} is not observed. Our assignment of Raman bands is summarized in Table I. We attribute two of the observed Raman modes at 440 cm^{-1} and at 1508 cm^{-1} to fundamental lattice vibrations. We assign the D and D^* features to disorder induced bands. The G band is attributed to deintercalated regions.

IV. DOUBLE RESONANCE RAMAN SCATTERING

Besides the fundamental Raman frequencies, spectra of CaC_6 exhibit features well known from disordered graphites¹⁰. These features are commonly labeled as

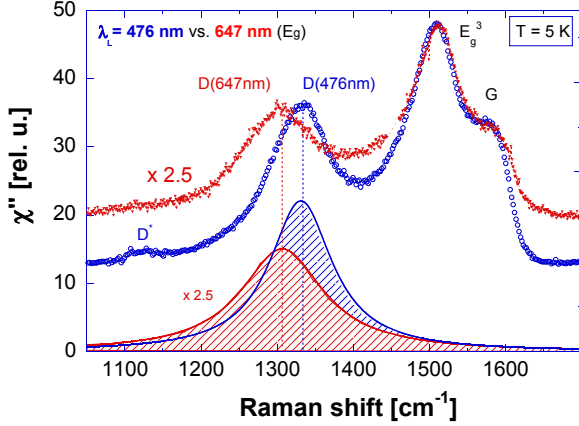


FIG. 3: (color online) CaC_6 Raman spectrum in the E_g symmetry channel excited with the 476 nm laser line (blue circles) vs. 647 nm (red triangles). The vertical scale of the 647 nm excitation spectrum has been adjusted for the E_g^3 mode to be displayed with the same relative intensity.

D and G bands and are identified by the rough frequency regions where they appear: around 1300 cm^{-1} for the D band and around 1600 cm^{-1} for the G band. The D band is indicative of disorder in form of scattering centers as found in polycrystalline samples²⁷, in highly-oriented pyrolytic graphite (HOPG) samples close to edges²⁸ and in irradiated graphite²⁹. The G band in graphite and graphene is attributed to the first order Raman band arising from the E_{2g} phonon, an in-plane hexagon compressing vibration. In few-layer graphene the position of the G band depends on doping of graphene sheets and on surface charges^{30,31,32}. We shall discuss the origin of the D and G band (shown in Fig-s 2 and 3) in this section.

The DRRS process couples to the disorder induced D band making points of the phonon dispersion away from the BZ center accessible by Raman scattering. By employing two excitation wavelengths we measure two such points by means of the D band Raman shift. More points in the phonon dispersion of CaC_6 will be traced with the help of other (weaker) disorder induced Raman bands³⁸. Fig. 3 shows how the D band shifts from 1308 cm^{-1} to 1332 cm^{-1} according to the excitation energy change from 647 nm to 476 nm. This translates to a frequency shift rate of $35 \text{ cm}^{-1} / \text{eV}$ in the visible light range of excitation energies in agreement with data presented in Fig. 1 of Ref.¹⁰. The observed frequency shift rate of the D band in CaC_6 is specific to this compound and is less than the 50 cm^{-1} frequency shift rate of the D band in graphite^{33,34} which allows

to attribute the observed D band to be specifically due to the DRRS in CaC_6 , excluding the scenario that we might be observing the graphitic D band from deintercalated regions.

The scheme for DRRS in CaC_6 (Fig. 4 a) involves graphene-derived electronic bands. There is a sequence of four steps to this process: (1) Following the absorption of the photon, an electron-hole pair is excited as a result of a real inter-band transition. This event occurs at the band wave vector k in the BZ, where the inter-band separation energy matches the excitation energy as indicated by a solid vertical arrow (AB for the blue laser line). If considering high-symmetry directions in the CaC_6 band structure, the inter-band transition for visible light is only possible at the wave vector k in the Γ -T direction of the rhombohedral BZ³⁹. This is why we chose the electronic band structure and the phonon dispersion along Γ -T to approximate our calculation of the DRRS effect in CaC_6 . (2) Next, the electron encounters an intra-band transition in which it is inelastically scattered by a phonon of a finite wave vector q opposite to the direction of the solid diagonal arrow (BC , for the blue laser light) that illustrates the electron transition. (3) The electron is elastically scattered back across the BZ (CD) by a defect to (4) recombine (DA) with the hole in the valence band by emission of the Raman shifted photon.

Fig. 4 a reveals two possible ways to inelastically scatter the electron in step 2 of the DRRS process: (a) Across the T point into the neighboring BZ between the two nonequivalent Γ points, namely in the Γ -T- Γ' direction (which is referred to as *inter-valley* scattering), or (b) across the Γ point between the right and left branches of the conduction band parabola inside the same BZ (which is referred to as *intra-valley* scattering). The D band frequency is determined by finding the phonon energy in the phonon dispersion that corresponds to the length of the phonon wave vector $|q|$, which is set by the second DRRS transition by either intra-valley or inter-valley scattering.

Fig. 4 b displays allowed DRRS frequencies as a function of excitation energy. We call this function a *double resonance curve*; there is one curve for each phonon branch and the set of the double resonance curves is unique for any material. The double resonance curve is obtained in two steps: (i) We examine the CaC_6 band structure and match the laser excitation energy to the electron wave vector k where the electron-hole pair creation can be accommodated by a corresponding energy separation between the electronic bands. This allows us to find the length of the phonon wave vector q involved in the inelastic scat-

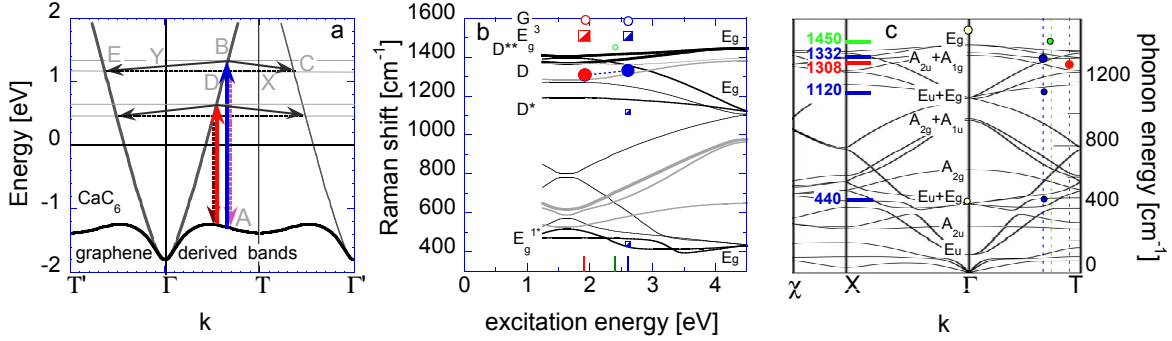


FIG. 4: (color online) Double resonance Raman scattering in CaC₆. *a*) Scheme of the DRRS process based on graphene derived electronic bands in CaC₆. The solid vertical arrows show the first resonant transition. The solid diagonal arrows show the second resonant transition in which the electron is scattered inelastically by phonons of finite wave vector q . The dashed horizontal lines indicate defect-induced elastic recoil of the electron. The vertical dashed lines depict the final electron-hole recombination. Both possible scattering scenarios: inter-valley (via T) and intra-valley (via Γ) are displayed. *b*) The solid lines show *double resonance curves*: allowed DRRS shifts a function of excitation energy. Lines in black are derived from 'E' branches and lines in grey from 'A' branches. DRRS curves derived from graphene like phonon branches (E_g³ and A_{2g}) are drawn with bold solid lines. All other (zone folded) curves are drawn either with simple solid lines when derived from even 'g' modes or with hair-lines for odd 'u' modes. The observed Raman peaks are marked by symbols at the respective excitation energies. The peak at 1450 cm⁻¹ is adopted from Ref. ¹⁰. *c*) The measured D, D*, D** and E_g^{1*}-bands positions are mapped in the CaC₆ phonon dispersion (adopted from Ref. ⁸) with colored and first order Raman active E_g modes with white circles.

tering step of the DRRS. (ii) We read off the phonon energy ω_q in the phonon dispersion that corresponds to the q -s obtained in the previous step for all possible excitation energies for selected phonon branches.

The conclusion is three-fold:

- (1) For CaC₆ there exists an activation threshold for the disorder induced DRRS process at 1.1 eV where the graphene derived conduction band crosses the Fermi level. This is in difference to DRRS in graphite where the first transition can in principle occur at arbitrary small excitation energies as a result of inter-band transitions between the Dirac cones in the proximity of the K points of the hexagonal BZ.
- (2) Because of the symmetry of the band structure the inter-valley and intra-valley scattering yield the same DRRS frequencies in the approximation that the length of the phononic wave vector q (which is the hypotenuse of the triangles BED and BDC) is estimated by the horizontal lines DE or DC⁴⁰.
- (3) The slope of the double resonance curves is positive for all three graphene derived phonon branches (thick solid lines) in the visible light range. Thus we expect a positive (blue) shift of the D band when the excitation energy is increased from 647 nm to 476 nm. The frequencies of observed Raman peaks are shown by symbols in Fig. 4 *b*. The position of the D band for the employed laser wavelengths is indicated by filled

circles. Considering the D band frequency range, its strong intensity and blue-shift of the D band with excitation energy, the DRRS characteristic displayed by the D band corresponds well to the double resonance curve derived from the lower E_g³ phonon branch. The experimental points are below the calculated curve by approximately 50 cm⁻¹. We conclude that the D band in CaC₆ originates from the lower E_g³ branch.

The D band is depolarized because phase information of the incoming photon is lost in the process of intra-band relaxational scattering. This is true for any DRRS induced band and thus two other depolarized features: at 1120 cm⁻¹ and at 440 cm⁻¹ (labeled D* and E_g^{1*}) may be interpreted as resulting from DRRS. These modes are marked by small symbols at their respective frequencies in Fig. 4 *b* and *c*. We find that E_g^{1*} is readily associated with the upper E_g¹ phonon branch that is mostly flat in the visible energy region. D* can arise from the lower E_g² phonon branch. It is 60 cm⁻¹ below the calculated double resonance curve. This error while substantial is of the same order as the error for the D band and appears to confirm what seems to be an overestimation of the phonon frequencies in the $\Gamma-T$ direction close to the edge of the BZ. Finally, we can treat the 1450 cm⁻¹ band that has been observed in Ref. ¹⁰ in CaC₆ samples exposed to air the same way. This band (labeled D** and represented by

a small circle at 2.41 eV in Fig. 4b) can be allocated to the highest double resonance curve originating from the upper E_g^3 branch. Indeed, examination of Fig. 1b of Ref. ¹⁰ shows that the 1450 cm^{-1} feature appears only along a very strong D band and is absent in spectra from freshly cleaved samples where the D band is weak. Consequently this peak can not be attributed to a Raman active mode but is a disorder induced DRRS band. The same argument holds also for the D^* band visible in Fig. 3 of Ref. ¹⁰. It confirms our interpretation of D^* as due to DRRS.

The frequencies of disorder induced bands can be plotted in the phonon dispersion diagram yielding a measurement for points of the phonon dispersion inside the BZ. The electronic band separation is in resonance with the red laser excitation of $\lambda_L = 647 \text{ nm}$ (1.917 eV) at $0.55 [\Gamma T]$ and with the blue excitation $\lambda_L = 476.4 \text{ nm}$ (2.604 eV) at $0.66 [\Gamma T]$, here $[\Gamma T]$ is the extension of the BZ in the respective direction. The corresponding resonant transition pairs (ω_{ph}, q_{ph}) are plotted for the frequencies of the disorder bands ω_{ph}^* in Fig. 4c. From these experimentally measured points of phonon dispersion we conclude that the calculation from first principles as performed in Ref. ⁸ underestimates the energy of the E_g^3 zone center mode, but tends to overestimate the energy of high frequency E_g branches close to the edge of BZ in the $\Gamma-T$ direction.

V. SUPERCONDUCTING GAP BY ELECTRONIC RAMAN SCATTERING

Below T_c low energy electronic Raman scattering exhibits a sharp SC coherence peak in the E_g symmetry channel at 24 cm^{-1} (Fig. 2 and Fig. 5c). The position of the coherence peak ($\sim 3.0 k_B T_c$) is in-between the values $2\Delta_{ab} = 21.8 \text{ cm}^{-1}$ reported from directional point contact spectroscopy¹⁷, where 'ab' refers to the direction of the current flow, and 25.8 cm^{-1} determined by STM measurements¹⁹.

The FWHM $\sim 12 \text{ cm}^{-1}$ of the coherence peak obtained by focusing the laser on a few 'high-quality' areas of the cleaved surface is of the same magnitude as the width of the step in the increase of reflectance below 2Δ observed in Ref. ²¹ and corresponds to the range of the anisotropic gap distribution suggested in Ref. ²⁰. But the characteristic width of the SC coherence peak and impurity related broadening will also contribute to the observed line width putting limits on possible gap distributions.

VI. THE EFFECT OF INTERCALANT DISORDER

Reactivity with air humidity poses a significant challenge to experimental investigation of CaC_6 . Previous spectroscopic work on lattice dynamics¹⁰ shows that Raman scattering is in particular sensitive to sample aging with the characteristic E_g^3 mode disappearing in less than half an hour upon air exposure. X-ray reflection study does not show comparable sensitivity¹¹. This makes Raman scattering a preferred method to probe surface degradation. When an imperfect spot on the sample surface is evaluated or when the sample is exposed to humidity in air the graphite-like D and G bands appear in the spectrum.

The disorder induced D band in graphite is associated with two main categories of defects. First, crystallite edges or domain boundaries^{27,28}, and second, defects introduced by ion irradiation²⁹ that can be understood as stray Coulomb potentials implanted in the crystal lattice. While comparison of the D and G band features in graphite to the D and G bands in CaC_6 can only be qualitative due to difference in crystal structure, some analogies to both types of disorder are observed. For polycrystalline graphites the relative Raman intensity ratio of the D band to the G band $I(D)/I(G)$ has empirically been found to increase linearly with the inverse crystallite size²⁷.

Substituting $I(G)$ of the Ref. ²⁷ calibration with $I(E_g^3)$ we find from Fig. 3 the ratio $I(D)/I(E_g^3) \approx 0.65$, which infers a hypothetical average domain size⁴¹ $L_a(\text{CaC}_6) \sim 100 \text{ \AA}$. This value is comparable with the mean free path of $\sim 500 \text{ \AA}$ along the ab -plane estimated from the residual resistivity of $\sim 1 \mu\Omega\text{cm}$. Additionally, this 'scale of disorder' is of the same magnitude as the superconducting coherence length $\xi \sim 300 \text{ \AA}$ as measured by scanning tunneling microscopy¹⁹. A similar $I(D)/I(G)$ intensity ratio is observed in annealed HOPG samples irradiated with ^{11}B ions²⁹ at a flux rate of $5 \times 10^{15} \text{ cm}^{-2}$. Intercalated Ca ions when displaced from their triangular pattern in the perfect crystalline order will have the effect of implanted stray Coulomb potentials in CaC_6 and will display a Raman signature that corresponds to the *micro-crystallite regime* described in Ref. ²⁹. This regime that is activated for ion fluences above $1 \times 10^{15} \text{ ions/cm}^2$ may be described as an intermediate state between the ordered and amorphous states when regions of disorder begin to coalesce/percolate forming islands of ordered regions surrounded by disorder. This state is reported to be metastable in graphite as the order can be restored by annealing. The line width of the partially polarized

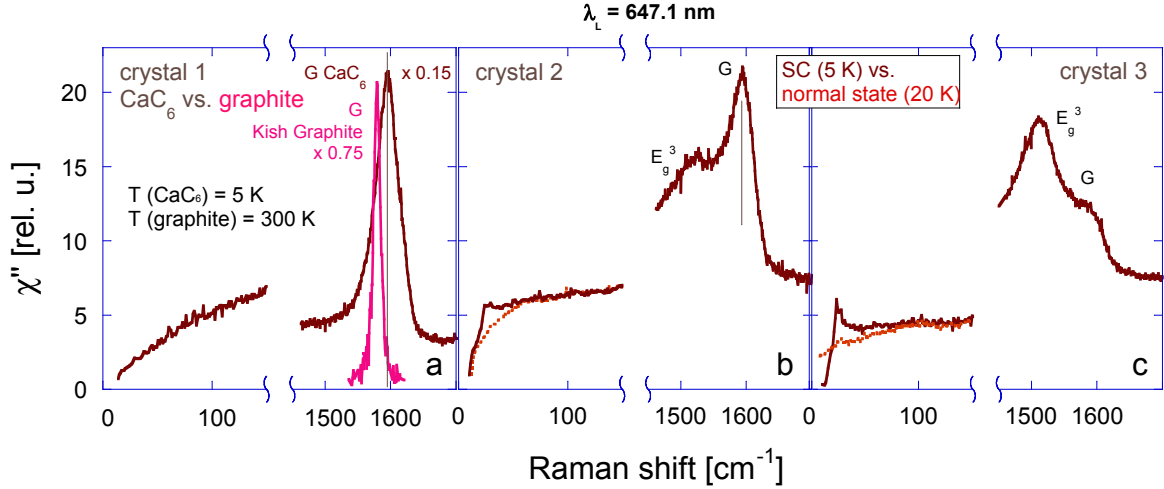


FIG. 5: (color online) The relative intensities of the E_g^3 mode (when present) and the G band in Raman spectra taken with the 647 nm excitation in RL geometry from different samples. *a*) No SC signature is observed in crystal 1, the E_g^3 mode is absent also. The pink solid line shows the RL polarized spectrum from kish graphite with its E_{2g} peak at 1579 cm^{-1} . *b*) The intensities of the the CaC_6 G band and the E_g^3 mode in crystal 2 relate approximately as 2:1. The superconducting coherence peak at 24 cm^{-1} is present but is weak and broad. *c*) The G band and E_g^3 intensities in crystal 3 relate approximately as 1:2. The strong E_g^3 mode and a sharp prominent SC coherence peak are at the same Raman shifts as in panel *b*).

G band in our CaC_6 sample ($\gamma_G = 32 \text{ cm}^{-1}$) also corresponds to the micro-crystallite regime of graphite damaged by ion implantation.

In general, a sharp pair breaking peak is observed by Raman in s-type superconductors in the clean limit³⁵. The relative intensity of the SC pair breaking peak to the background allows evaluation of the SC properties. There is a distribution of results ranging from absence of any SC features in the Raman spectrum (Fig. 5 *a*) to a sharp, well pronounced SC coherence peak (Fig. 5 *c*). Broadening and vanishing of the SC coherence peak is attributed to different degrees of disorder caused by possible Li-ion contamination, Ca deintercalation or aging of the cleaved surface. The shown spectra represent the best results obtained from a set of spots identified by a visual scan of the respective crystals surfaces.

In Fig. 5 we show that the relative ratio of the E_g^3 mode intensity to that of the G band correlates with the width and intensity of the SC coherence peak. We evaluate Raman scattering in the low energy window up to 150 cm^{-1} to trace the SC signature and in the high energy window between 1450 cm^{-1} and 1700 cm^{-1} for the phononic signature. Both measurements are performed on the same spot of the cleaved surface and in the same cooling cycle. Sample 1 (Fig. 5 *a*) displays a smooth, close to linear slope at low energies showing no SC peak at all. Correspondingly, at high Raman

shifts the unique E_g^3 phononic mode of CaC_6 is absent with only the G band contributing to the Raman intensity. We therefore suggest that down to the skin depth the CaC_6 structure is disturbed from its rhombohedral form by Ca deintercalation. We compare the CaC_6 G band to the graphitic G band recorded from a kish graphite sample to find that in the deintercalated CaC_6 the G band is upshifted in comparison to simple graphite. This might reflect remnant doping by 'surviving' disordered Ca atoms but should not be interpreted as a sign of electron-phonon coupling in CaC_6 as without the E_g^3 mode at 1508 cm^{-1} it is not an ordered CaC_6 structure any more. Sample 2 (Fig. 5 *b*) shows weak superconductivity with a broad SC pair breaking peak on top of underlying background intensity. In this case we do observe the E_g^3 mode with about half the intensity of that of the G band. The investigated region of sample 2 is superconducting but can be described as *low quality*. The respective shapes and relative intensities of recorded electronic/phononic Raman modes are characteristic of contamination. Sample 3 (Fig. 5 *c*) displays a sharp SC pair breaking peak, its rhombohedral structure is intact with the E_g^3 mode more than two times stronger than the G band. We characterize this sample as *high quality/ low contamination* crystal. In summary, for sample quality evaluation purpose the relative intensity of the E_g^3 mode to the CaC_6 G band

indicates if the sample in question is superconducting. The E_g^3 mode must be present for superconductivity to occur and the greater its intensity relative to the G band arising from deintercalated regions the greater portion of the sample is superconducting.

VII. CONCLUSION

In conclusion we have investigated polarized Raman spectra from CaC_6 samples with different degree of disorder. The best of the examined samples exhibits a clear signature of superconductivity in the form of a SC coherence peak at 24 cm^{-1} . We have used this sample to record detailed first order Raman scattering spectra. In these spectra we have identified two fundamental E_g modes and additional graphite like D and G bands re-

sulting from disordered and partially non-intercalated regions. The dispersive behavior of the D band as a function of excitation energy is a signature of double resonant Raman scattering in CaC_6 . We have calculated double resonance curves for all phonon branches. On the basis of this calculation we have assigned the D band to result from the lower E_g branch along the Γ -T line of the CaC_6 phonon dispersion. By using different laser excitations we have measured points in the phonon dispersion at finite wave vectors. From analogies to studies of disordered graphites the investigated CaC_6 samples are best described as being in a microcrystallite regime with domain boundaries $\sim 100 \text{ \AA}$.

We thank F. Mauri and I. Mazin for discussion. AM acknowledges support by Rutgers University, the Alcatel-Lucent Foundation and the German Academic Exchange Service.

-
- ¹ M. Dresselhaus and G. Dresselhaus, *Advances in Physics*, **30** (1981).
 - ² G. Csanyi, P.B. Littlewood, A. Nevidomskyy, C. Pickard, and B. Simons, *Nature Physics* **1** 42, (2005).
 - ³ I. Mazin, L. Boeri, O. Dolgov, A. Golubov, G. Bachelet, M. Giantomassi, and O. Andersen, *Physica C* **460** 116 (2007).
 - ⁴ T. Weller, M. Ellerby, S. Saxena, R. Smith and N. Skipper, *Nature Physics* **1** 39 (2005).
 - ⁵ N. Emery, C. Hérold, and P. Lagrange, *J. of Solid State Chem.* **178**, 2947 (2005).
 - ⁶ N. Emery, C. Hérold, M. d'Astuto, V. Garcia, Ch. Bellin, J. F. Marêché, P. Lagrange, and G. Loupías, *Phys. Rev. Lett.* **95** 087003 (2005).
 - ⁷ J. S. Kim, L. Boeri, R. K. Kremer, and F. S. Razavi, *Phys. Rev. B* **74**, 214513 (2006).
 - ⁸ M. Calandra and F. Mauri, *Phys. Rev. Lett.* **95**, 237002 (2005).
 - ⁹ D. G. Hinks, D. Rosenmann, H. Claus, M. S. Bailey, and J. D. Jorgensen, *Phys. Rev. B* **75** 014509 (2007).
 - ¹⁰ J. Hlinka, I. Gregora, J. Pokorný, C. Hérold, N. Emery, J. F. Marêché, and P. Lagrange, *Phys. Rev. B* **76**, 144512 (2007).
 - ¹¹ M. H. Upton, A. C. Walters, C. A. Howard, K. C. Rahnejat, M. Ellerby, J. P. Hill, D. F. McMorrow, A. Alatas, Bogdan M. Leu, and Wei Ku, *Phys. Rev. B* **76**, 220501(R) (2007).
 - ¹² A. M. Saitta, M. Lazzeri, M. Calandra, and F. Mauri, *Phys. Rev. Lett.* **100**, 226401 (2008).
 - ¹³ A. H. Castro Neto, *Nature Materials* **6** 176, (2007).
 - ¹⁴ R. Martin and L. Falicov, *Light Scattering in Solids I* (2nd ed.), 79 (1983).
 - ¹⁵ C. Thomsen and S. Reich, *Phys. Rev. Lett.* **85**, 5214 (2000).
 - ¹⁶ R. Saito, A. Jorio, A. G. Souza Filho, G. Dresselhaus, M. S. Dresselhaus, and M. A. Pimenta, *Phys. Rev. Lett.* **88** 027401 (2001).
 - ¹⁷ R. S. Gonnelli, D. Daghero, D. Delaude, M. Tortello, G. A. Ummarino, V. A. Stepanov, J. S. Kim, R. K. Kremer, A. Sanna, G. Profeta, and S. Massidda, *Phys. Rev. Lett.* **100** 207004 (2008).
 - ¹⁸ C. Kurter, L. Ozyuzer, D. Mazur, J. F. Zasadzinski, D. Rosenmann, H. Claus, D. G. Hinks, and K. E. Gray, *Phys. Rev. B* **76** 220502(R) (2007).
 - ¹⁹ N. Bergeal, V. Dubost, Y. Noat, W. Sacks, D. Roditchev, N. Emery, C. Hérold, J. F. Marêché, P. Lagrange, and G. Loupías, *Phys. Rev. Lett.* **97**, 077003 (2006).
 - ²⁰ A. Sanna, G. Profeta, A. Floris, A. Marini, E. K. U. Gross, and S. Massidda, *Phys. Rev. B* **75** 020511(R) (2007).
 - ²¹ U. Nagel, D. Hüvonen, E. Joon, J. S. Kim, R. K. Kremer, and T. Rööm, *Phys. Rev. B* **78**, 041404(R) (2008).
 - ²² R. Loudon, *Advances in Physics* **13**, 423 (1964).
 - ²³ A. Pinczuk and E. Burstein, *Topics in Applied Physics* **8**, *Light Scattering in Solids I (2nd Edition)*, 23 (1983).
 - ²⁴ N. Kambe, M. S. Dresselhaus, G. Dresselhaus, S. Basu, A. R. McGhie, and J. E. Fischer, *Material Science and Engineering* **40** 1 (1979).
 - ²⁵ P. C. Eklund, G. Dresselhaus, M. S. Dresselhaus, and J. E. Fischer, *Phys. Rev. B* **16** 3330 (1977).
 - ²⁶ A. Solin, *Physica B* **99** 443 (1980).
 - ²⁷ F. Tuinstra and J. L. Koenig, *The Journal of Chemical Physics* **53** 1126 (1970).
 - ²⁸ L. G. Cançado, M. A. Pimenta, B. R. A. Neves, M. S. S. Dantas, and A. Jorio, *Phys. Rev. Lett.* **93** 247401 (2004).
 - ²⁹ B. S. Elman, M. S. Dresselhaus, G. Dresselhaus, E. W. Maby and H. Mazurek, *Phys. Rev. B* **24** 1027 (1981).
 - ³⁰ J. Yan, Y. Zhang, P. Kim and A. Pinczuk, *Phys. Rev. Lett.*

- 98** 166802 (2007).
- ³¹ A. Gupta, G. Chen, P. Joshi, S. Tadigadapa, and P. C. Ek-
lund, *Nano Letters* **6**, 2667 (2006).
- ³² H. Son , A. Reina , M. S. Dresselhaus, and Jing Kong, *The
G-band phonon frequency in single layer graphene*, APS
March Meeting 2008, Session B28.00009:
- ³³ R. P. Vidano, D. B. Fishbach, L. J. Willis, and T. M. Loehr,
Solid State Commun. **39**, 341 (1981).
- ³⁴ M. J. Matthews, M. A. Pimenta, G. Dresselhaus,
M. S. Dresselhaus, and M. Endo, *Phys. Rev. B* **59**,
R6585 (1999).
- ³⁵ M. V. Klein and S. B. Dierker, *Phys. Rev. B* **29**, 4976
(1984).
- ³⁶ R. Narula and S. Reich, *Phys. Rev. B* **78**, 165422 (2008).
- ³⁷ The B_{2g} out of plane graphene vibration becomes an A_{2g}
vibration in CaC_6 . Both are silent modes.
- ³⁸ We observe these weak disorder modes only with the
476 nm excitation. These modes are apparently below the
noise floor in the 647 nm spectra.
- ³⁹ The Raman amplitude is going to be resonant in a region
around this point involving large BZ areas of low symme-
try in the DRRS as illustrated in Fig. 6 of Ref.³⁶. Limiting
the discussion to the high symmetry directions of the BZ
suffices for the purpose of demonstrating the origin of the
disorder induced bands.
- ⁴⁰ $q = BC = 2 - 2k = q' = BE$, where q and q' are
the phonon wave vectors for inter-valley and intra-valley
scattering respectively. $q' > 1$, requiring extension of the
phonon dispersion into the neighboring BZ along $|\Gamma - T|$.
- ⁴¹ With 6 C atoms in the ab -cross section of the CaC_6 unit
cell vs. 2 atoms in the primitive cell of a graphene layer
the linear characteristic length in CaC_6 scales as $\sqrt{3}$ in re-
spect to that of graphite, resulting in a $70 \text{ \AA} \times \sqrt{3} \approx 120 \text{ \AA}$
estimate for $L_a(\text{CaC}_6)$.